Water-Immersed Microwave Antennas and Their Application to Microwave Interrogation of Biological Targets

JOHN H. JACOBI, MEMBER, IEEE, LAWRENCE E. LARSEN, AND CHARLES T. HAST, MEMBER, IEEE

Abstract—**This paper describes a method of significantly improving the resolution of systems used for interrogating the spatial variation of permittivity of biosystems at *S* band. The basic principle employed is to contract the wavelength of the interrogating radiation and to reduce the physical aperture of the interrogating probes by immersing the transmitting antenna, receiving antenna, and the target into a material with a high dielectric constant, namely water. The antenna design is described, and line scans employing transmitted and reflected energy are presented.**

I. INTRODUCTION

THERE ARE many forms of radiation that are used today for noninvasive exploration of biosystems. The active systems include X-ray, radioneucliotides, and heavy particle, neutron, and ultrasonic imaging systems. Passive thermographic systems have also been developed which depend upon the Planck distribution of emitted radiation whose spectrum is a function of body temperature. These systems include infrared and microwave thermographic measurement devices [1]–[6].

Active imaging systems which employ electromagnetic radiation with a wavelength greater than 3 mm have not been developed for use in biosystems due to a number of apparent limitations. At shorter wavelengths in the microwave region, where spatial resolution of an imaging system would be best, the attenuation of energy as it passes through water-dominated dielectrics is so great that the detection of transmitted energy is not practical or possible. The same problem is encountered in the detection of reflected energy with the difficulty increasing as the reflecting boundary resides at deeper ranges within the body. Obviously, it is possible to overcome the attenuation problem by simply operating at a lower frequency. The demise of this scheme is that as the frequency is reduced the wavelength of the radiation increases and the physical aperture of the antenna needed to efficiently deliver the interrogating energy also increases. In the case of microwave interrogation, this results in the degradation of spatial resolution of the system to the point where it becomes useless as an imaging system. Clearly then, there are compromises between spatial resolution and loss of signal.

Another problem which plagues microwave interrogation systems is multipath propagation. If one attempts to measure the transmission loss and phase shift through a lossy dielectric in a nonanechoic environment, it is likely that the majority of the signal reaching the receiving antenna has not passed through the object of interest. Rather, it has been reflected into the receiving antenna from a surface exterior to the body, or the wave has been guided around the body into the receiving antenna. Yamaura [7] has performed experiments on humans at *S* band and demonstrates that multipath is a serious problem. He was not able to obtain useable results unless the antennas were in contact with the body. This means that in order to make high-quality measurements, one should perform them in an anechoic environment. Obviously, operating in an anechoic environment does not alleviate the problem of multipath internal to the body under study. This problem is effectively addressed with other methods such as microwave time-delay spectroscopy or pulsed RF techniques.

Finally, there is the problem of the dielectric discontinuity encountered at the air-skin interface. Because of the difference between the dielectric constants of air and skin [8], there will be a large reflection of the incident energy at this interface.

All of the problems presented above would seem to make the idea of an active microwave imaging system for biological targets a hopeless endeavor. However, an approach has been devised which has the fortuitous quality of providing significant relief for all of the problems described. The idea is to transmit and receive with antennas that operate totally immersed in a semi-infinite space of water. The object under examination would then be immersed in the water space between the two antennas.

In the last twenty-five years, considerable interest has been shown in underwater transmission of electromagnetic waves. The main impetus for these efforts has been the possibility of underwater communications. Most of the past investigations have been limited to VHF frequencies and below. Baños [9] presents a very rigorous mathematical analysis of dipole radiation in a conductive medium. To simplify the complex mathematics, he

Manuscript received June 2, 1978; revised September 1, 1978.

J. H. Jacobi and L. E. Larsen are with the Walter Reed Army Institute of Research, Washington, DC 20012.

C. T. Hast is with the American Electronic Laboratories, Incorporated, Lansdale, PA 19446.

0018-9480/79/0100-0070$00.75 ©1979 IEEE

assumed only low-frequency characteristics. King and his associates have performed considerable work on electrically insulated water-immersed dipoles [10]–[12] and compared their results to Baños' equation. In a later paper [13], radiation patterns of a submerged VHF antenna were presented.

The present effort requires the subsurface transmission of energy at microwave frequencies. Little mathematical analysis or experimental investigation has been performed in this frequency range, and at present there is a gap in our knowledge of submerged transmission between VHF and light frequencies where geometric optical theories can be applied.

The resolution of diffraction-limited imaging systems is determined by the wavelength of the interrogating radiation. That is, wavelength and spatial resolution are inversely related. In the case of microwave near-field imagery, resolution can be considered in terms of the physical aperture of the transmitting and receiving antennas. When operating in the near field of an antenna, the spatial resolution of the imaging system monotonically improves with decreases in aperture size. The relative permittivity of pure water at 3 GHz is 76.7. Therefore, the velocity of propagation and the wavelength is reduced by $\sqrt{76.7}$. Because of the contraction in wavelength, the physical area of an open-ended waveguide antenna that can be matched to the intrinsic impedance of the medium over a broad bandwidth is reduced by a factor of 76.7. Thus, by operating the transmitting and receiving antennas completely submerged in and filled with water, one can achieve significant improvement in the spatial resolution of the interrogating system for near-field imagery.

The need to operate the interrogating system in an anechoic chamber is completely eliminated by immersing the entire system in water. Water is such a lossy medium (382 dB/m at 3 GHz) that energy radiated towards the top, bottom, and sides of the water tank is attenuated to an undetectable level before it reaches the reflecting surfaces in tanks of practical sizes. In a sense, the water space appears as if it had infinite dimensions, and the enviornment is inherently anechoic.

Finally, there is the improvement of energy coupling into the body due to the presence of the water. The dielectric constant of skin is much more closely matched to water than it is to air. Therefore, the reflections at the water-skin interface are much less than they would be at an air-skin interface. Also, water hydrates the corified epithelium and improves the impedance match at the 100–200 microns of the skin which would otherwise be very low in water content. There are two major benefits to the reduced reflection at the interface. The most obvious one is improved efficiency of the interrogating system. As the coupling of the energy to the body is improved, then one can expect higher energy levels at the receiving antenna. One could achieve the same effect by dielectric surface-matching techniques in which the antennas would contact the skin or by tuning stubs, but the resulting system would be cumbersome. The second benefit is connected with processing of signals reflected from internal interfaces such as the muscle-bone interface. A large reflection at the air-skin interface imposes a requirement of greater dynamic range and sensitivity on the microwave receiving system in order to be able to detect reflections from internal boundaries. To the extent that this large reflection can be eliminated, examination of reflections from internal interfaces can be simplified. Note, however, that the reflection at the skin should not be entirely eliminated. This is desirable in order to preserve an important reference point, the surface of the body.

II. Methods

A. Antenna Design

This research program required an antenna which would operate under water at frequencies from 2 to 4 GHz. The basic reasons for the large bandwidth are that it is desirable to use methods in addition to continuous wave (CW) interrogation for characterizing the dielectric target. The methods include microwave time-delay spectroscopy and pulsed microwave interrogation techniques. The antenna was designed to operate in distilled water at 32 °C. A temperature of 32 °C (slightly above room temperature) was selected so that the bath temperature could be regulated with only a heater. A bath at room temperature would have required a heater and refrigeration unit for regulation. The use of water as a transmission media presents two major problems: very high dielectric constant and extremely high transmission loss. Experimental values for the relative permittivity and loss tangent of water have been extensively tabulated [14]–[16]. The average relative permittivity from 2 to 4 GHz is 77. An antenna loaded with such a material would need to be reduced to the size of an antenna operating in free space from 18 to 36 GHz.

Standard waveguide to coaxial adapters have been used, both at the Walter Reed Army Institute of Research and the American Electronic Laboratories as narrowband underwater radiators. These transitions have been used at L band without modification of the design, only waterproofed and size reduced to account for the dielectric loading. In order to obtain octave bandwidth, a double-ridged waveguide to coaxial adapter was selected as the prototype antenna.

Various attempts were made to match an unmodified transition to a 50-Ω impedance while it was submerged in water. The adapter performed very well in free space from 18 to 36 GHz, but underwater from 2 to 4 GHz the match was worse than 7:1 across the band. It appeared that the waveguide probe was not operating in the lossy media. To obtain better control over the larger impedance the probe was shorted to the far ridge of the waveguide. This lowered the VSWR to better than 4:1 across the 2–4-GHz band.

A maximum loss of 3 dB per antenna had been established as a project goal. To meet this goal, it was apparent that the antenna had to be reduced to a length of ap-

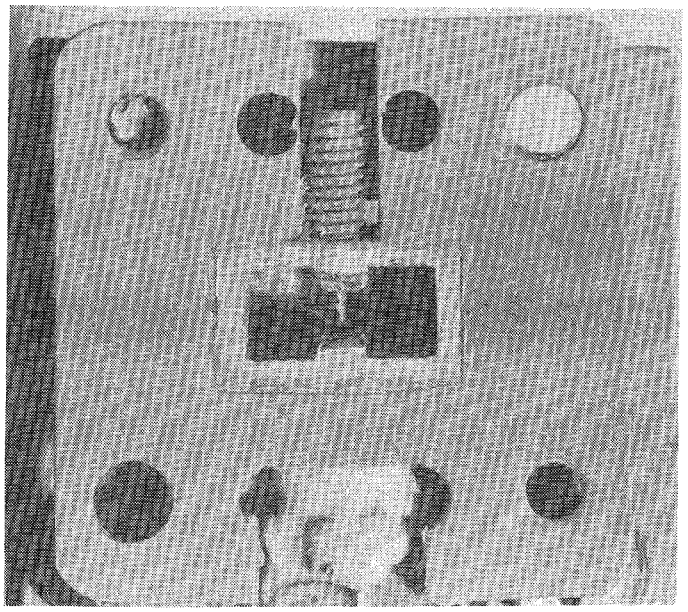

Fig. 1. Frontal view of completed antenna.

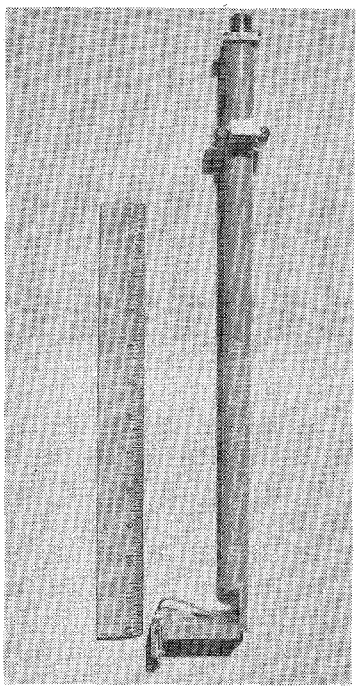

Fig. 2. Completed antenna assembly.

proximately 3 mm because of the high losses in the water-filled waveguide. An antenna this short would not permit the use of tuning screws for impedance matching. A length of 6.7 mm was selected as a good compromise between internal loss and ease of matching.

Matching of the antenna across the octave bandwidth required careful adjustment of a number of parameters. The diameter of the feed probe was reduced to 0.5 mm to provide a better match to the high-impedance ridges of the waveguide. The spacing between the back shorting plate and the feed probe was adjusted to obtain the smoothest impedance match from 2 to 4 GHz. Two holes, size 2-56, were drilled and tapped into the bottom ridge of the waveguide. Tuning screws, placed into these holes, were used to obtain a broader match. Final matching of the antenna was obtained by simultaneous adjustment of the two tuning screws and the penetration into the cavity of the feed probe's TEFLON® dielectric. The antenna performed best when the dielectric was just even with the waveguide's inside surface. Because of the relatively high temperature coefficient of expansion of the TEFLON®, it was important that the final adjustments be performed at the maximum operating temperature, 32°C. The slight contraction of the dielectric at lower water temperatures does not adversely affect the antenna's impedance match.

The antenna was enclosed in a standard double-ridged waveguide flange. The flange provided mechanical stability and a method of mounting extensions onto the antenna. The flange was machined to permit the installation of the feed cable onto the input connector and access for adjustment of the tuning screws. A 2.2-mm-diameter hole was drilled in the shorting plate. This hole permits easy air-bubble removal from the antenna and can be used as a sight to help align the antenna on the target. There is very little radiation from this hole since it is below cutoff for this frequency band. Fig. 1 is a frontal view of the final antenna showing the flange and the open end of the ridged waveguide. The probe can be seen between the ridges. The hole for removing air bubbles is directly behind the probe. Beneath the probe is one of the tuning screws for impedance matching.

The completed antenna was supported at the end of a tube 45 cm long. The hollow tube supports the antenna and protects the feed cable which is terminated in a type-*N* connector at the top of the tube. To reduce the effect of any reflections off the tube, the antenna was held 5 cm in front of the tube by a metal standoff. An adjustable clamp holds the tube and permits the antenna to be positioned at any height or angular position. A photograph of the final antenna assembly and its supports is shown in Fig. 2.

To measure the combined internal losses of two antennas, a set of swept transmission loss measurements were taken. The antennas were tested centered in a 56.8-l glass tank with 10-cm depth of 32°C distilled water. First, a reference plot was taken by making a through connection without the antennas. Then the cables were reconnected to the antennas, and another plot of loss was made with the antenna flanges touching. The difference between this data and the reference plot is an estimate of the internal insertion losses of the two antennas including feed cables and connectors.

When using the antennas for imagery, it is of interest to know the distance to the far field. To insure that the imagery experiments were done in the near field, a series of antenna patterns were taken at various antenna spacings. The antennas were submerged to a middepth of 10 cm in 32°C distilled water. One antenna was held stationary while the second was rotated. A synchro on the rotator was used to drive a standard polar chart recorder. The stationary antenna was used as a transmitter while

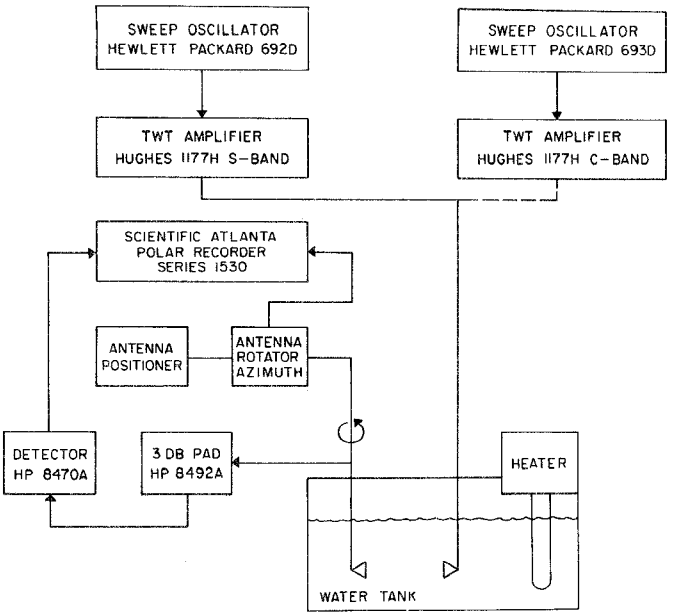

Fig. 3. Antenna pattern measurement test configuration.

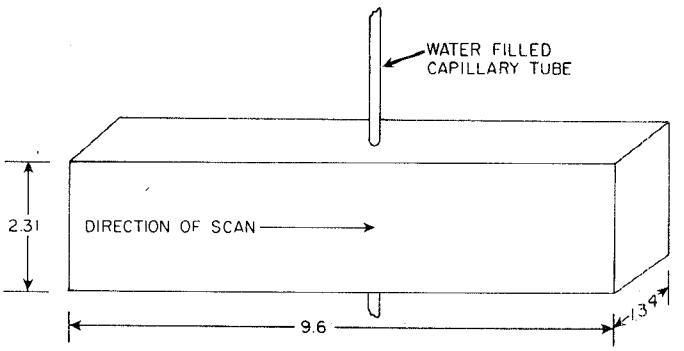

Fig. 4. Sketch of vessel in fat model.

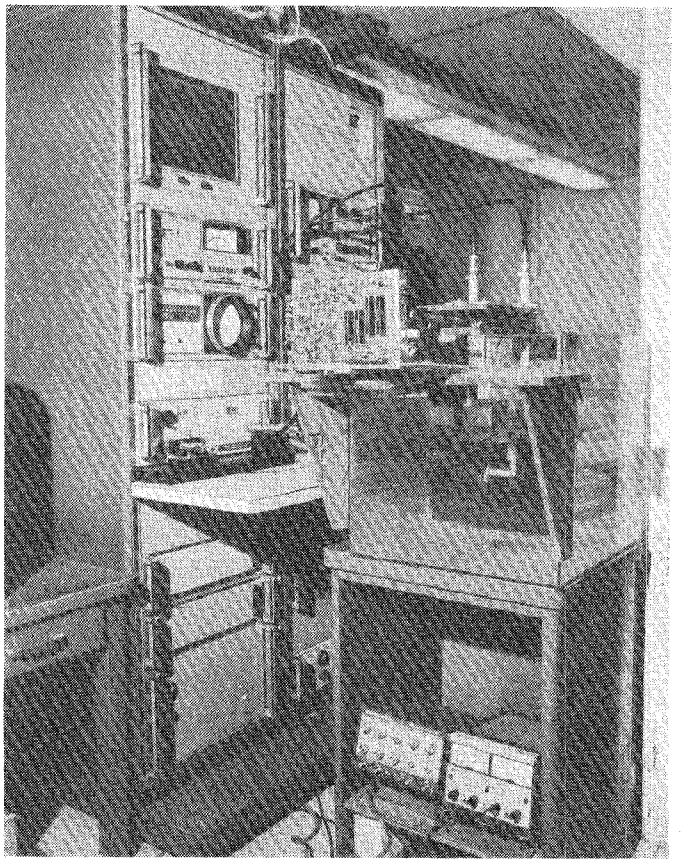

Fig. 5. Experimental arrangement for imaging experiment.

the output from a crystal detector on the other antenna was used to drive the pen position of the recorder. Fig. 3 is a block diagram of the test setup used for these measurements. Because of the extreme RF losses in the water, it was very important to place the center of the antenna aperture at the center of rotation of the positioner. In air, antenna patterns are generally taken with the antenna's phase center on the center of rotation. If this were done under water, the pattern would be distorted due to the difference in path losses as the antenna was rotated.

B. Line Scan Experiment

To experimentally verify the spatial resolution properties of the system, a set of experiments involving dielectric targets of increasingly complex geometry were devised. Two sets of experiments were performed in order to obtain a qualitative understanding of the response of underwater antennas to dielectric targets of simple geometry. Each experiment had two phases: single targets and then double targets. In the first set of experiments with the water-loaded antennas, they were immersed in water spaced 6.8 mm apart. The targets were air-filled capillary tubes 1.8 mm in diameter oriented with their long axis parallel to the electric field. The antenna pair was scanned in a direction orthogonal to the direction of propagation and in such a manner that the targets passed midway between the two antennas. A Hewlett–Packard 8542A automatic network analyzer (phase-locked version) was used to measure the magnitude and phase of the reflection coefficient (S_{11}) of the transmitting antenna and the magnitude and phase of the transmission coefficient (S_{21}) between the two antennas. All of the measurement data shown in this section was taken at 3.999 GHz. The reason for this choice of frequency was so that the system could be studied under conditions of maximum spatial resolution. The scattering parameters were measured as a function of position as the antennas were moved relative to the target. The first phase of the first experiment used a single capillary tube as a target. The second phase of the first experiment used a pair of tubes at three different spacings: 5, 10, and 15 mm. The second experiment also consisted of two parts, a single water-filled capillary tube embedded in simulated fat [17] and then two tubes spaced 10 mm apart embedded in simulated fat. In this second experiment, the antenna spacing was increased to 2.25 cm in order to accommodate the thickness of the fat. Again, the long axis of the capillary tube was parallel to the electric field and the scan was orthogonal to the direction of propagation. A drawing of the simulated fat model with one capillary tube in place is shown in Fig. 4.

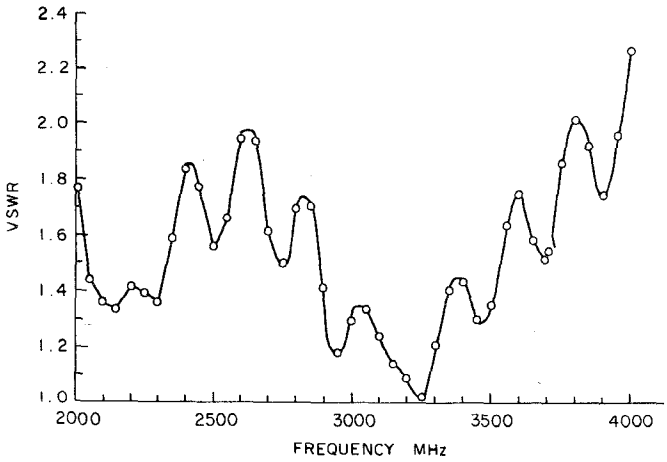

Fig. 6. VSWR of antenna submerged in water.

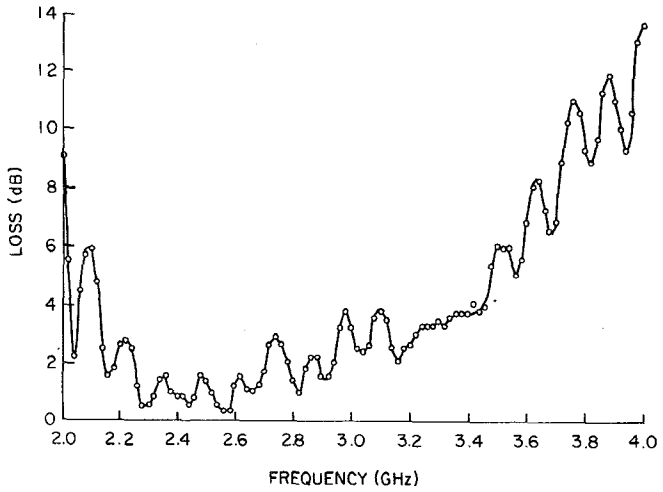

Fig. 7. Combined insertion loss of two antennas, interconnecting cables and connectors.

Fig. 5 is a photograph of the experimental arrangement. The automatic network analyzer is in the cabinets in the background. In front of the analyzer is the water tank with the two antennas in place. The water tank is a cube, 45.7 cm on a side. It was filled to within 6.4 cm of the top, and the antennas were immersed 17.8 cm below the surface of the water. The positioning of the antennas was controlled by the same computer that controlled the network analyzer. After each measurement of the scattering parameters, the computer issued a sequence of pulses to control a stepper motor that drove a micrometer on the antenna positioner. With this system, the minimum step between antenna positions was 0.0025 mm. The circuit board shown attached to the water tank is the stepper motor logic control circuitry.

III. Results

A set of measurements on two production antennas was performed at the American Electronic Laboratories antenna facility. These initial measurements were to prove the performance of the antennas and define their general operating characteristics. While the data presented is by no means a complete analysis of the antennas, it does demonstrate the basic antenna characteristics.

Fig. 6 is a plot of the VSWR of the completed antenna operating submerged in water. As shown on the plot, a match of better than 2:1 was obtained for this particular antenna up to approximately 3.96 GHz. This result is presented as typical since the VSWR varies as a function of the cleanliness of the antenna and the degree to which small air bubbles can be removed from the vicinity of the probe in the center of the waveguide.

The combined insertion loss of the two antennas is shown in Fig. 7. In order to avoid high transmitted powers or extreme receiver sensitivity, the design goal was a combined loss of 6 dB. This goal was met over approximately 79 percent of the total desired band. Even at the highest frequency, the total loss for both antennas is only 14 dB which is still acceptable for this application.

The beamwidth of the underwater antenna was measured at several different antenna spacings. Fig. 8 is a

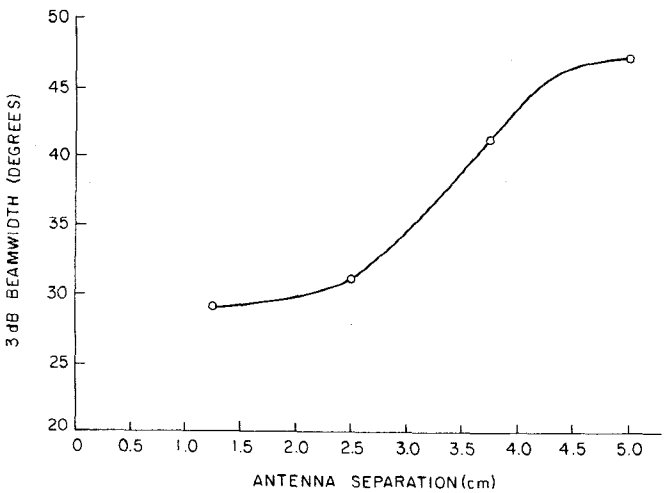

Fig. 8. Beamwidth variation versus spacing: $F=3000$ MHz.

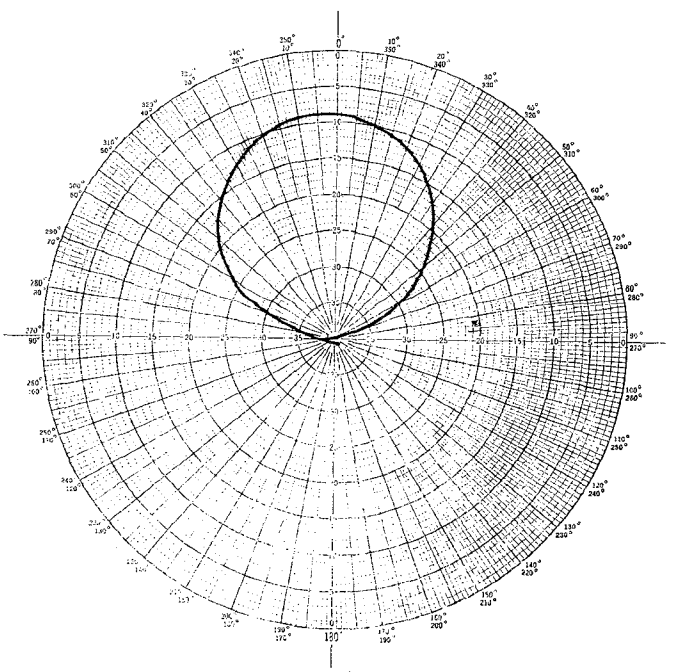

Fig. 9. Pattern at 3000 MHz. Distance between antennas is 5.1 cm.

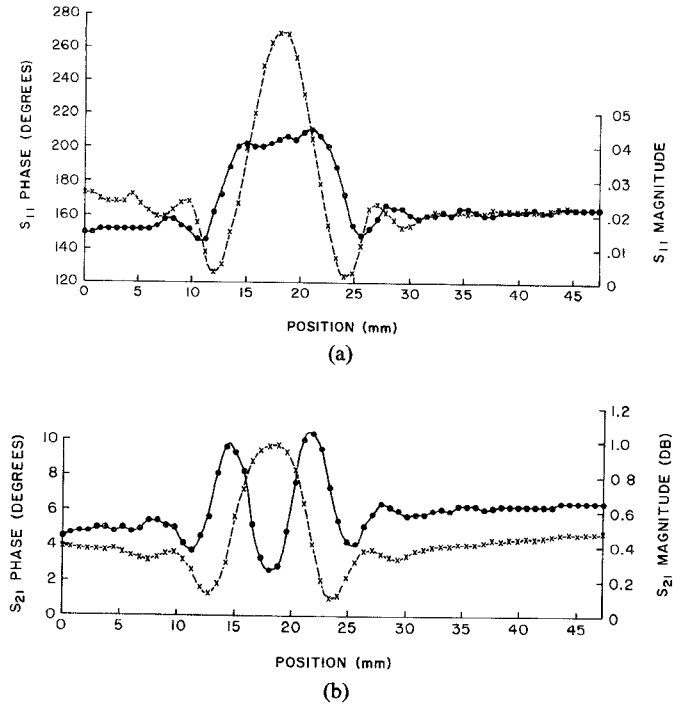

Fig. 10. Single air-filled capillary tube in water. (a) Reflection coefficient. (b) Transmission coefficient. Solid lines are magnitude; dashed are phase.

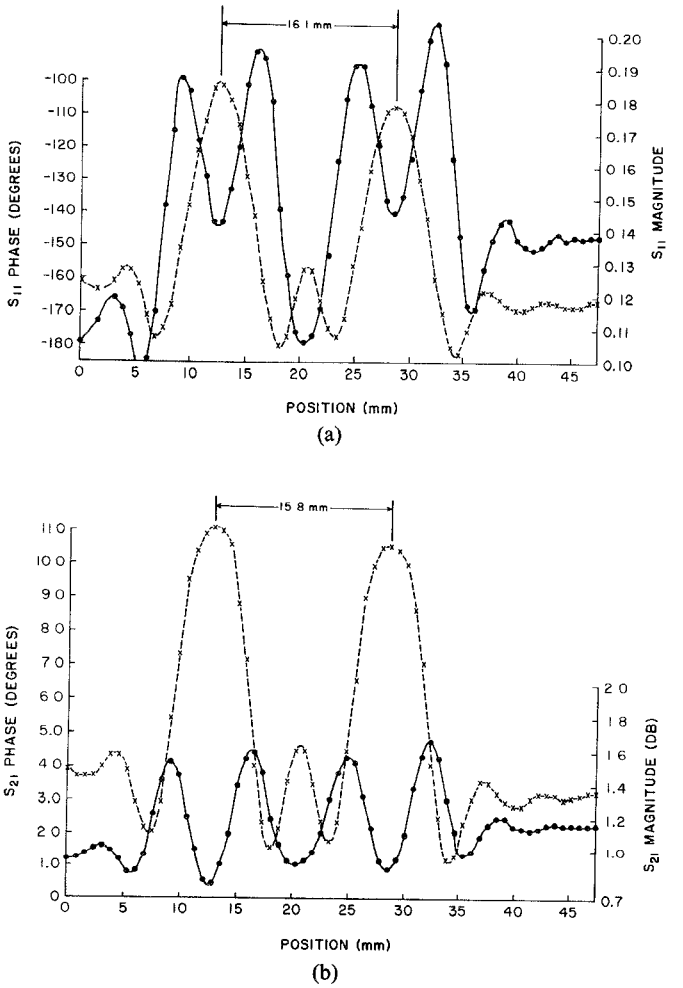

Fig. 11. Two air-filled capillary tubes in water. Spacing = 15 mm. (a) Reflection coefficient. (b) Transmission coefficient. Solid lines are magnitude; dashed are phase.

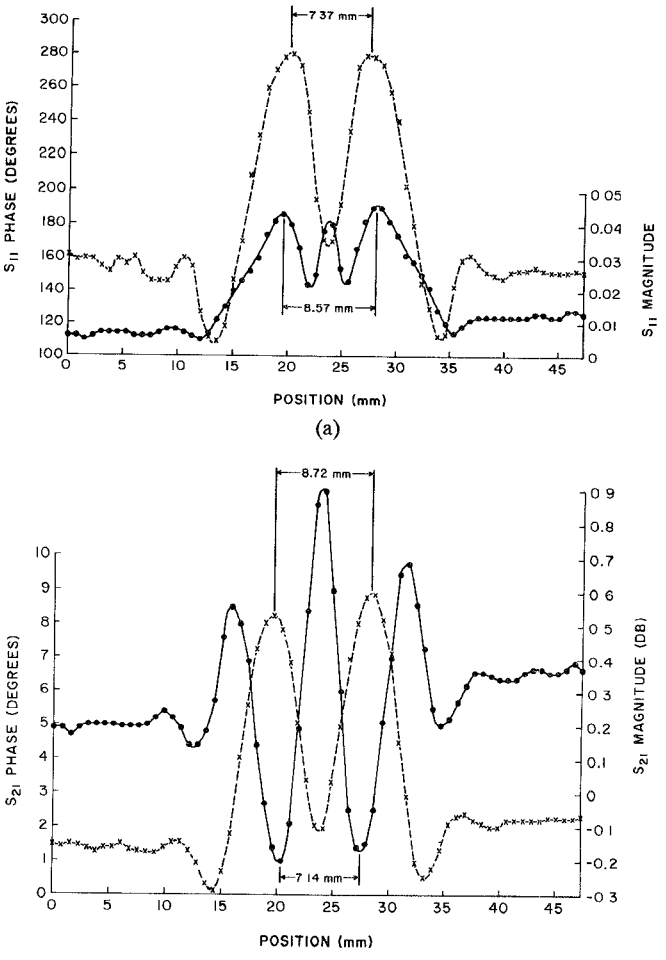

Fig. 12. Two air-filled capillary tubes in water. Spacing = 10 mm. (a) Reflection coefficient. (b) Transmission coefficient. Solid lines are magnitude; dashed are phase.

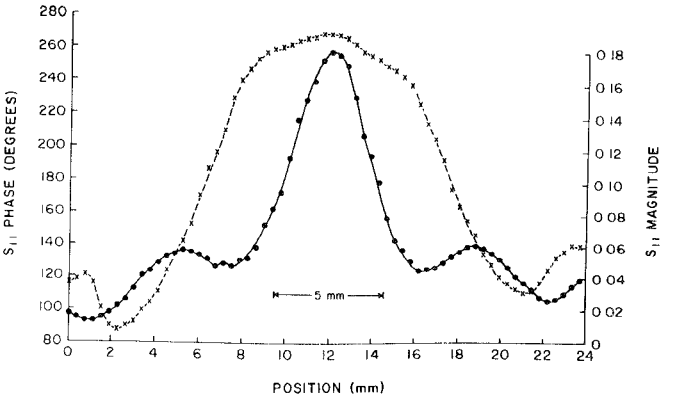

Fig. 13. Two air-filled capillary tubes in water. Spacing = 5 mm. Reflection coefficient. Solid line is magnitude; dashed is phase.

plot of beamwidth at 3 GHz at antenna spacing from approximately 1–5 cm. The pattern at a frequency of 3 GHz and a spacing of 5.1 cm is shown in Fig. 9.

The following figures present the imagery qualities of the antennas in scattering parameter data. Fig. 10 shows the magnitude and phase of the scattering parameters for the case of a single air-filled capillary tube immersed in water. Figs. 11–13 present scattering parameter data for two capillary tubes in water spaced at 15-, 10-, and 5-mm

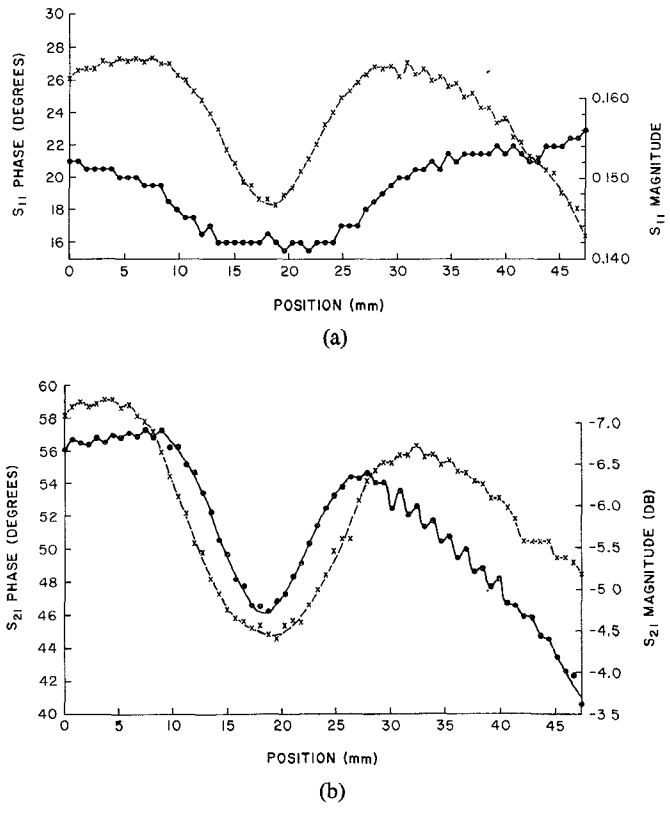

Fig. 14. Single water-filled capillary tube in simulated fat. (a) Reflection coefficient. (b) Transmission coefficient. Solid lines are magnitude; dashed are phase.

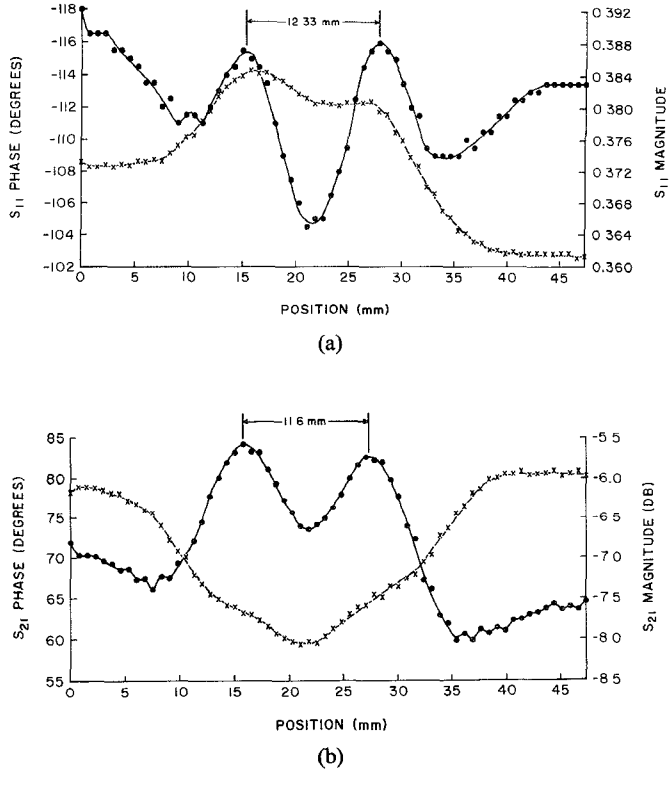

Fig. 15. Two water-filled capillary tubes in simulated fat. Spacing = 11 mm. (a) Reflection coefficient. (b) Transmission coefficient. Solid lines are magnitudes; dashed are phase.

separations. Fig. 14 shows the scattering parameter data for a single water-filled capillary tube embedded in simulated fat. Fig. 15 depicts the results for two water-filled capillary tubes spaced 11 mm apart in simulated fat.

IV. Discussion

There were several major design objectives for the water-loaded antennas. They had to exhibit small physical size compared to the free-space wavelength in order to provide adequate spatial resolution for biologically relevant targets. Despite their small size, the antennas had to perform efficiently over approximately one-octave bandwidth so that they could be used with pulsed or swept interrogating radiation. Finally, the antennas had to operate completely submerged in water so that the advantages of that environment could be realized. The combined loss data shown in Fig. 7 and the VSWR data shown in Fig. 6 serve to illustrate that these performance features are achievable.

The magnitudes and phases of both S_{11} and S_{21} for a single capillary tube in water (Fig. 10) are clear indicators of the presence of the target, changing rapidly as the target begins to enter the opening of the waveguide. The presence of standing waves are clear in all the functions, and, as expected, this behavior persists in the presence of multiple targets in the water.

The response of the scattering parameters for two 1.8-mm diameter capillary tubes separated by 15 mm is shown in Fig. 11. The peaks in the phase of both S_{11} and S_{21} are clear indicators of the position of the two capillary tubes. There is a slight filling in the trough between the peaks of the phase functions indicating that the responses of the two targets are beginning to interact slightly at this spacing. The magnitudes of both S_{11} and S_{21} are already beginning to exhibit strong standing-wave patterns, and, by themselves, these functions would not provide much information about target size or location. The indicated separation of the targets is within 1.1 mm of the expected value. This error was within the limit of our capability to position the capillary tubes relative to each other.

At the 10-mm separation (Fig. 12), the phase of both S_{11} and S_{21} continue to indicate the presence of two separate targets. However, the proximity of the two is such that the interaction between the two targets has made the peak of the phase functions an inaccurate indicator of the position of the targets. The phase of S_{21} is the more accurate of the indicators of target position differing from the expected value by approximately 15 percent.

At the 5-mm separation (Fig. 13), the distinction between the two targets is completely gone. The data for S_{21} is not shown because it is equally uninformative.

When a single target embedded in simulated fat (Fig. 14) is displayed by its scattering parameters, three of the functions give a clear indication of the location of the capillary tube. The magnitude of S_{11} is very noisy and gives only a weak response. The rapidly varying standing-wave patterns previously observed in water have disap-

peared due to the expanded wavelength in fat. In this medium, the wavelength is approximately 3.3 cm.

When two capillary tubes are embedded in fat (Fig. 15), the distance between the tubes inferred by the peaks in the magnitude of S_{11} and the troughs in the magnitude of S_{21} are in good agreement with the measured distance between the tubes. The distance between the two tubes was 11 mm. The distance indicated by the separation in the peaks in the magnitudes of S_{11} and S_{21} are 11.6 and 12.33 mm, respectively.

In evaluating these results, one should bear in mind that the width of the flange of the antenna is 22.2 mm and the width of the broad dimension of the waveguide is 7.7 mm. Examination of this data indicates that noticeable effects on the scattering parameters begins to occur about the time that the target encroaches upon the edge of the flange of the antenna. Even though the response does begin to appear at that point, it is clear that there is significant resolution within the opening of the waveguide. For example, the phases of both S_{11} and S_{21} in Fig. 10 rise rapidly as the target begins to enter the area of the opening of the waveguide. The magnitude of S_{11} is rather flat in the region of the opening of the waveguide.

The imaging experiments demonstrate that very high resolution in space is possible with small apertures. It was shown that objects spaced approximately 10 mm apart (13 percent of the free-space wavelength) produced clear and separate responses in the measured scattering parameters. A very important conclusion in connection with this is that one cannot depend upon a single variable (e.g., phase of S_{21}) for location of target inhomogenities. For example, in Fig. 15 the phase of S_{21} provides practically no information at all; on the other hand, in Fig. 11 the phase of S_{21} is quite informative. The point is that all four parts of the scattering parameter data must be considered in formulating an image. It appears that the limit of resolution for the system operating in the near field of the antenna is approximately equal to the width of the broad dimension of the waveguide opening. Here, we are defining resolution as the ability to distinguish two separate point targets. One can easily see from Figs. 12 and 15 that targets spaced by 10 mm produce separate responses. Fig. 13 shows that when the target spacing is less than the broad dimension of the waveguide, then the two targets are indistinguishable.

There are numerous examples in the data of standing-wave patterns. One would expect that the distance between a peak and valley in the standing-wave pattern would be some multiple of a quarter-wavelength in water. The wavelength at 3.999 GHz in water is 8.55 mm. In most cases, the distances between the peaks and valleys are considerably removed from the expected value. The discrepancy is probably due to the complex arrangements of reflectors and materials of varying dielectric constants in the vicinity of the antenna. It will be the subject of future investigations. The high-frequency standing-wave patterns on the fat/vessel model are presumably due to mechanical instability in the scanning apparatus. This conclusion is reached because the peaks and valleys lie exactly on the increments taken by the scanner.

The question of accuracy of the positioning mechanism is shown to be extremely important. The experiments showed that phase changes on the order of 35°/mm exist in S_{11}. The accuracy of measurement of the phase of S_{11} by the 8542A network analyzer is approximately $\pm 1.0°$. In order to make the errors introduced by the mechanical scanner small (i.e., 0.1°), the positioning accuracy must be on the order of $(0.1°)\ (1\ \text{mm}/35°) = 2.86 \times 10^{-3}$ mm.

Detection of dielectric constant discontinuities within otherwise homogeneous dielectrics was shown with the simulated fat/water-filled capillary tube model. One particularly interesting result of this experiment is the fact that the spacing between the two capillary tubes agreed quite closely with the distance between the peaks in the scattering parameters. This was not the case with the two tubes separated by 10 mm in water. It is likely that this result is due to the fact that the longer wavelength in the fat extended the distance between the peaks in the standing-wave pattern and thus eliminated the ability of standing waves to interfere with the image.

V. Conclusions

In this paper, we present experimental evidence that it is practical to construct a simple antenna that operates at *S* band while completely submerged in water. This antenna has good impedance characteristics (VSWR < 2.3) and reasonable losses (less than 14-dB total for two antennas) over an octave from 2 to 4 GHz. To the best of our knowledge, this is the first successful attempt to operate transmitting and receiving antennas underwater at these frequencies.

It is demonstrated that it is possible to use these antennas to create line scan images of dielectric targets. Objects with a diameter of 1.8 mm and spacing of 10 mm are easily detected by interrogating radiation whose wavelength is 75 mm. The resolution of the system (in terms of separating two closely spaced objects) is shown to lie between 5 and 10 mm. The data also shows that the presence of multiple dielectric discontinuities does not destroy the ability of the system to resolve closely spaced objects. This is demonstrated in the vessel-in-fat model.

References

[1] B. Enander and G. Larson, "Measurements of thermal electromagnetic radiation from the human body at microwave frequencies," Division of Electromagnetic Theory, The Royal Institute of Technology, Stockholm, Sweden, TRITA-TET-7602, Mar. 1976.

[2] A. H. Barrett and P. C. Myers, "Subcultaneous temperatures: A method of noninvasive sensing," *Sci.*, vol. 190, pp. 669–671, 1975.

[3] J. Edrich and P. C. Hardee, "Thermography at millimeter wavelengths," *Proc. IEEE*, vol. 62, pp. 1391–1392, Oct. 1974.

[4] B. Enander and G. Larson, "Microwave radiometric measurements of the temperature inside a body," *Electron. Lett.*, vol. 10, p. 317, July 1974.

[5] ——, "Measurements of thermal electromagnetic radiation from the human body at radio frequencies," Division of Electromagnetic Theory, The Royal Institute of Technology, Stockholm, Sweden, TRITA-TET-7505, Dec. 1975.

[6] J. Bigu del Blanco, C. Romero-Sierra, and J. A. Tanner, "Some theory and preliminary experiments on microwave radiometry of biological systems," presented at 1974 IEEE/GMTT Int. Microwave Symp., Atlanta, GA., June 1974, in *IEEE Symp. Rec.* (no. 74CHO 838-3 MTT), pp. 41–43.
[7] I. Yamaura, "Measurements of 1.8–2.7-GHz microwave attenuation in the human torso," *IEEE Trans. Microwave Theory Tech.*, vol. MTT-25, pp. 707–710, Aug. 1977.
[8] H. P. Schwan, "Radiation biology, medical applications, and radiation hazards," *Microwave Power Engineering*, vol. 2, E. C. Okress, Ed. New York: Academic, 1968, pp. 215–232.
[9] A. Baños, Jr., *Dipole radiation in the presence of a conducting half-space.* New York: Pergamon, 1966.
[10] M. Siegel and R. W. P. King, "Radiation from linear antennas in a dissipative half-space," *IEEE Trans. Antennas Progagat.*, vol. AP-19, pp. 447–485, July 1971.
[11] T. T. Wu, L. C. Shen, and R. W. P. King, "The dipole antenna with eccentric coating in a relatively dense medium," *IEEE Trans. Antennas Propagat.*, vol. AP-23, pp. 57–62, Jan. 1975.
[12] R. W. P. King, S. R. Mishra, K. M. Lee, and G. S. Smith, "The insulated monopole: Admittance and junction effects," *IEEE Trans. Antennas Propagat.*, vol. AP-23, pp. 172–177, Mar. 1975.
[13] L. C. Shen, R. W. P. King, and R. M. Sorbello, "Measured field of a directional antenna submerged in a lake," *IEEE Trans. Antennas Propagat.*, vol. AP-24, pp. 891–894, Nov. 1976.
[14] C. G. Montgomery, R. H. Dicke, and E. M. Purcell, *Principles of Microwave Circuits.* New York: Dover, 1965.
[15] J. A. Saxon, "Dielectric dispersion in pure polar liquids," *Royal Soc. of London Proc.*, series A, vol. 213, no. 1115, p. 478, 22 July 1952.
[16] A. R. von Hippel, "Tables of dielectric materials," in *Dielectric Materials and Applications*, A. R. von Hippel, Ed. New York: Wiley, 1954, p. 361.
[17] C. C. Johnson and A. W. Guy, "Nonionizing electromagnetic wave effects in biological materials and systems," *Proc. IEEE*, vol. 60, pp. 692–718, June 1972.

A Microwave System for the Controlled Production of Local Tumor Hyperthermia in Animals

RICHARD L. MAGIN, MEMBER, IEEE

Abstract—**A microwave system was designed and constructed which provides controlled, localized hyperthermia in the tumors of four experimental animals. The components of the system are a 2.45-GHz microwave source, a four-way power-dividing network and reflected power monitor, a temperature-controlled microwave power regulator, and small direct-contact microwave applicators. Adjustment of the temperature control results in elevated temperatures in the centers of tumors which can be maintained to within ± 0.1°C without production of significant whole body hyperthermia. The temperatures at the edges of the locally heated tumors were found to vary within ± 1.0°C of the center temperature. The system is currently being used to evaluate the therapeutic potential of sustained localized hyperthermia in small tumors implanted subcutaneously in mice.**

I. Introduction

THERE IS continuing interest within the cancer-research community in the application of hyperthermia as an adjuvant to ionizing radiation and drug therapies [1], [2]. Both laboratory and clinical studies are proceeding to establish the efficacy of this combination treatment. The effects of local tumor hyperthermia can be investigated using small animal tumor models. These models have the advantages of well-characterized growth patterns and known sensitivities to drugs and other antitumor agents. In order to study the effectiveness of heat in treating these animal tumor models, it is necessary to develop an apparatus which produces a controlled and localized tumor hyperthermia.

Several techniques have been employed by previous researchers to use microwaves for the local heating of tumors. Gessler *et al.* [3], Allen [4], and Yerushalmi [5] used metallic screens to shield the bodies of mice and rats, restricting the microwave exposure from microwave diathermy applicators (types A and C) to the area of the tumor. Copeland and Michaelson [6] also used a metallic screen to shield the body of a rat, while the tumor was drawn through a hole cut in the screen. The entire rat was then irradiated with 2.80-GHz microwaves from an *H*-plane sectoral horn antenna. Robinson *et al.* [7] improved on these methods by simultaneously forcing warm air over the surface of the tumor during microwave exposure resulting in more uniform intratumor temperatures. Cater *et al.* [8] localized the exposure to the tumor by suspending tumor bearing thighs of rats in front of a waveguide (7.0×3.5 cm) operating at 3.00 GHz. Zimmer *et al.* [9] used direct-contact microwave applicators at 2.45 and 9.05 GHz to rewarm the local tumor areas of hypothermic

Manuscript received April 27, 1978; revised August 14, 1978. This research was conducted in the Laboratory of Chemical Pharmacology, National Cancer Institute, Bethesda, MD 20014.

The author is with the Department of Radiation Biology and Biophysics, University of Rochester, Rochester, NY.